

Article

Mechanical Properties and Crack Classification of Basalt Fiber RPC Based on Acoustic Emission Parameters

Hanbing Liu ¹, Shiqi Liu ¹, Peilei Zhou ^{1,*}, Yuwei Zhang ¹ and Yubo Jiao ²

¹ College of Transportation, Jilin University, Changchun 130025, China; lhb@jlu.edu.cn (H.L.); sqliu17@mails.jlu.edu.cn (S.L.); ywzhang@jlu.edu.cn (Y.Z.)

² Key Laboratory of Urban Security and Disaster Engineering of Ministry of Education, Beijing University of Technology, Beijing 100022, China; jiaoyb@bjut.edu.cn

* Correspondence: zhoupeilei@jlu.edu.cn; Tel.: +86-133-4140-0976

Received: 25 August 2019; Accepted: 17 September 2019; Published: 19 September 2019



Abstract: The workability and mechanical properties of basalt fiber reactive powder concrete (BFRPC) were investigated by univariate analysis. The acoustic emission (AE) was used as a non-destructive technique to reveal the damage characterization of concrete samples of varying basalt fiber content. The fracture stages and modes of specimens during flexural test were determined by AE parameters. The content of silica fume, quartz sand and basalt fiber of 0.4, 1.3 and 10 kg/m³, respectively, was found related to optimal improvements in mechanical strength. As for the characteristics of fracture, it was found that the fiber content was a significant determinant, and the key AE parameters, namely, hits, energy and amplitude, were found related to the damage stage of specimens. Furthermore, rise time (RA) and average frequency (AF) were found to have opposite trends during loading while their variation related to the fracture modes of BFRPC.

Keywords: reactive powder concrete; basalt fiber; acoustic emission; mechanical properties; crack classification

1. Introduction

The concept of ultra-high performance concrete (UHPC) appeared in the 1990s [1], and one of the most widely used is Reactive Powder Concrete (RPC). As a new class of cement-based material, RPC has become the focus on developing cement materials due to its great strength, high tenacity and outstanding durability [2,3]. Traditional RPC improves the homogeneity and compactness of the matrix by eliminating coarse aggregate and adding active constituents such as silica fume and fly ash [4]. This ultra-compact microstructure results in low permeability and high durability. Previous studies have verified that the compressive strength of RPC can reach 200–800 MPa, together with the ultimate tensile strain on the order of 1% [5]. To further enhance the performance, steel fibers are commonly chosen for reinforcement to promote the ductility and the flexural strength of RPC [6]. Nowadays, RPC is considered as a promising material for use in special pre-stressed and precast concrete components. Although the production cost of RPC is generally high, its ultra-high mechanical properties make it possible to reduce the thickness of concrete members, which results in reducing material consumption. Therefore, it also has economic advantages in practical application.

Basalt fiber has been used for many years as a reinforcing material in concrete technology. This fiber is a kind of environmental protection material with high performance and is made of natural basalt. Due to its high tensile strength, excellent elastic modulus and superior corrosion resistance, basalt fiber is a beneficial admixture for concrete.

The addition of steel fiber in RPC not only affects the production costs, but also has negative effects on the dead load and may cause corrosion problems [7]. Replacing steel fibers with basalt fibers seems to be a feasible solution to these problems [8]. In addition, incorporation of basalt fibers may positively impact the workability of concrete. Branston et al. [9] found that, when the mass content reaches 12 kg/m^3 , the strengthening effect of basalt fiber on the flexural strength and impact strength of concrete is similar to that of steel fiber. It has been validated that the addition of 0.15% basalt fiber and 0.033% polypropylene fiber can increase the flexural and compressive strength of high-performance concrete by 14.1% and 22.8%, respectively [10]. Ayub et al. [11] found that the maximum compressive strength could reach 84.08 MPa with a volume content of 2% basalt fiber in UHPC when 10% cement was replaced by silica fume and kaolin.

The damage of concrete materials including matrix cracking and the fracture caused by fiber pulling out. If the fracture processes and cracking patterns of concrete can be determined, the structure can be strengthened with appropriate design to enhance the resistance to specific fracture patterns. Meanwhile, it would lead to an early warning to final fracture. Nowadays, there is a technique that has shown enormous potential for real-time monitoring and evaluation of material damage called acoustic emission (AE). The acoustic emission is a non-destructive testing (NDT) technique with the advantages of high sensitivity and full period online monitoring [12]. In recent years, AE technology has been widely used in the construction field, such as crack monitoring and damage assessment of reinforced concrete beam [13], shear wall [14] and short wall [15]. Previous studies have shown that the AE generated by solid fracture is similar to the propagation mode of seismic waves. In reference to the Gutenberg–Richter empirical relation in seismology, the b-value method can be adopted to analyze AE data [16]. Siracusano et al. [17] established the damage assessment system of fiber-free concrete by Hilbert–Huang Transform processing of AE data, verifying the role of AE technology in the monitoring and health assessment of infrastructure service status. AE technology can also locate the internal damage of the structure. Mhamdi et al. [18] compared two AE source location approaches by breaking lead test on the steel plates, verifying the accuracy of AE localization. Aggelis et al. confirmed that the average frequency, rise angle and other characteristic parameters of AE are significantly correlated with the internal damage of materials [19].

In this study, the mix proportion of basalt fiber reactive powder concrete (BFRPC) based on the single-variable optimization method using simple tests was developed. The research aimed to apply basalt fiber in the production of RPC, so as to reduce the material costs and ensure the workability. Furthermore, BFRPC specimens were subjected to flexural test with coinstantaneous recording of the AE events. The ultimate load and AE parameters were measured as a function of the fiber content. The fracture process and cracking mode were also related with the fiber content. Additionally, the characteristic parameters of AE signals could act as a forerunner of damage, which verified the applicability of AE method in high-performance material structure.

2. Acoustic Emission Method

AE signals refer to elastic waves whose energy attenuates from high order to low order, which are generated due to the internal damage of materials and obtained by sensors attached to the surface of materials [20]. The number of AE signals obtained in the monitoring process is related to material properties, damage process and intensity [16]. Meanwhile, the value of AE characteristic parameters depends on the intensity of local damage. Therefore, AE technology can reveal the failure process and fracture mode of materials so that it can be used for health monitoring of concrete structures.

Typical AE signals and characteristic parameters collected by AE measurement system are shown in Figure 1. The threshold level set by users is a key parameter of AE testing. A reasonable threshold can eliminate the influence of environmental noise on the accuracy of data and reflect the actual cracking of materials [21,22]. Amplitude (A) is the maximum voltage corresponding to the peak of signal waveform and measured in decibels (dB). Rise time (RT) is the time interval from when the signal first crosses the threshold until it reaches the maximum value. AE energy is the elastic energy

released by AE events, which is considered as quantification of the intensity of damage. AE count is the number of times the signal amplitude crosses the threshold value. Duration is the time interval between the first and last crossing of the signal and threshold, which is measured in microseconds (μ s).

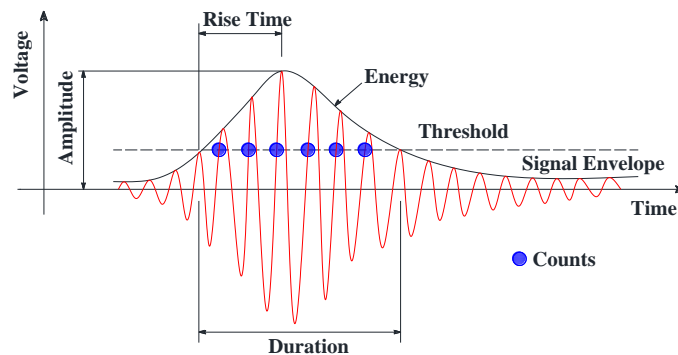


Figure 1. Typical acoustic emission signals and parameters.

To classify the cracks of concrete, the RA value and average frequency (AF) are proposed based on the JCMS-III B5706 code, and defined by Equations (1) and (2).

$$RA\ value = \frac{Rise\ Time}{Amplitude},\ ms/V \tag{1}$$

$$Average\ frequency\ (AF) = \frac{Counts}{Duration},\ kHz \tag{2}$$

It has been found that there are differences in signal waveforms under different fracture modes [23]. Tensile events are characterized by higher AF and lower RA values than shear events. This is mainly because the energy released by tensile crack appears in the form of longitudinal wave, which propagates faster than shear wave, with high amplitude and short rise time. Shear events release energy mainly in the form of shear waves, the slower wave velocity leads to longer rise time and duration [24]. Therefore, the fracture mode of materials can be determined through the analysis of RA-AF value. Typical signal waveforms under different fracture modes are shown in Figure 2.

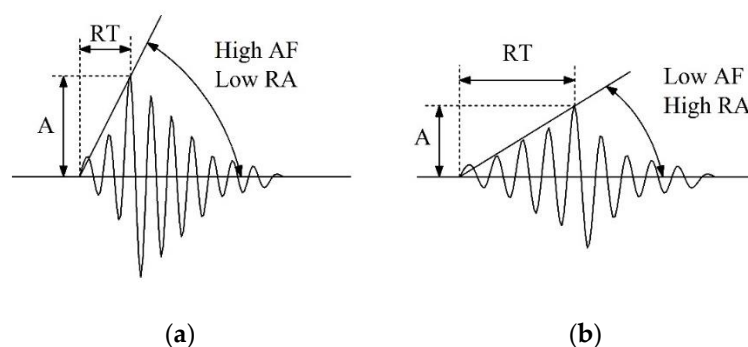


Figure 2. Acoustic emission (AE) signals of different fracture mode: (a) tensile mode; and (b) shear mode.

3. Experimental Details

3.1. Materials

Portland cement (type P. II 52.5) manufactured by Yatai Cement Co., Ltd., Jilin, was used in this study. The silica fume was a type of SF93 silica produced by Si’ao Technology Co., Ltd., Changchun, which had a mass fraction of 93.3% and a specific surface area of 18100 m^2/kg . Three sizes of quartz sand produced in Zhenxing quartz sand factory, Luoyang, were used in this study, namely mesh

sizes of 30–45, 45–100 and 100–150, with the proportion of 2:4:1. HPWR-Q8011 poly-carboxylic based superplasticizers (SP) produced by Qinfen Building Materials Co., Ltd., Shanxi were used in all tested concretes. The chopped basalt fiber used in this study was 22 mm length and 23 μm diameter, produced by Anjie Composite Material Co., Ltd., Haining with a tensile strength of 2836 MPa and elastic modulus of 62 GPa. The pertinent chemical and physical properties of the cement, SF, basalt fiber and quartz sand used in this study are given in Tables 1–3.

Table 1. Chemical compositions of cement and silica fume.

Items	Chemical Compositions (%)					
	SiO ₂	Al ₂ O ₃	Fe ₂ O ₃	CaO	MgO	SO ₃
Cement	22.6	5.6	4.3	62.7	1.7	2.5
Silica fume (SF)	93.3	0.73	0.49	0.85	1.21	1.02

Table 2. Properties of basalt fibers.

Fiber Type	Length (mm)	Diameter (μm)	Linear Density (tex)	Tensile Strength (MPa)	Elastic Modulus (GPa)	Breaking Strength (N/tex)	Elongation (%)
Basalt fiber	22	23	2392	2836	62	0.69	3

Table 3. Chemical compositions of quartz sand.

Component	SiO ₂	Fe	Al ₂ O ₃	K ₂ O	Na ₂ O	H ₂ O
Content (%)	99.68	0.0062	0.0122	0.0011	0.002	0.02

3.2. Mixture Proportions and Sample Preparation

Table 4 shows the proportions of BFRPC prepared in this study. The ratios of water/binder (W/B), silica fume/cement (SF/C), quartz sand/cement (QS/C) and the content of basalt fiber (BF) were set as variables with three levels each. All BFRPC mixtures were produced using a mortar mixer of ISO 679 (JJ-5). Initially, quartz sand and basalt fiber were mixed for about 2 min. The dry powders (cement and SF) were then added and mixed for 3 min. Subsequently, the water and superplasticizer were added in two batches, mixing for 3 min each time. The mixture was poured into metallic oiled molds, with volumes of 40 mm \times 40 mm \times 160 mm, immediately after mixing, three for each group, and compacted by vibrating on the vibrator table (ZT-96). After being cast, the specimens were kept in the molds for 24 h at 95% RH and 20 °C and then demolded. They were subsequently heat treated in HH-6 thermostatic water tank at 60 °C. The curing lasted for 48 h, with initial heating rate of 12 °C/h and final cooling rate of 15 °C/h.

Table 4. Mix proportions of basalt fiber reactive powder concrete (BFRPC). W/B, water/binder; SF/C, silica fume/cement; QS/C, quartz sand/cement; BF, basalt fiber.

Mix	W/B	SF/C	QS/C	Materials (kg/m ³)					
				Cement	SF	QS	Water	SP	BF
BF1	0.18	0.4	1.6	769	308	1230	194	97	10
BF2	0.2	0.4	1.6	762	308	1230	215	97	10
BF3	0.22	0.4	1.6	756	308	1230	237	97	10
BF4	0.2	0.2	1.3	756	154	999	185	83	14
BF5	0.2	0.4	1.3	912	308	999	215	97	14
BF6	0.2	0.6	1.3	839	461	999	246	111	14
BF7	0.2	0.4	1.0	776	308	769	215	97	10
BF8	0.2	0.4	1.3	933	308	999	215	97	10
BF9	0.2	0.4	1.3	839	308	1230	194	97	6

3.3. Testing

The fluidity of fresh mixture was evaluated by the jumping table method described in the Chinese Standard JTG E30-2005 [25]. The flexural strength was evaluated according to the standard GB/T 17671-1999 [26]. For each mix proportion, three specimens of 40 mm × 40 mm × 160 mm were prepared for testing, with loading rate of 50 N/s. The compressive strength was evaluated in accordance with the standard GB/T 17671-1999 [26]. For each group, six fracture blocks acquired in the flexural test were used for compressing, with a constant loading rate of 2.4 kN/s.

In the flexural test, the SAEU2S-6 acoustic emission acquisition and analysis system produced by Shenghuaxingye Technology Co., Ltd., Beijing was used to monitor the flexural failure process of specimens. An AE sensor with signal sampling frequency of 5 MHz was fixed on the side of specimen through an elastic fixation band. The Vaseline was used as coupling agent to couple the sensor with the surface of sample to eliminate the air between the interfaces, and the lead breaking test was used to ensure the AE sensor was coupled well [27]. The AE experiment arrangement for flexural test is shown in Figure 3. To filter the environment and machine noise, the threshold of AE detection was set to 60 dB, and the acquisition frequency of AE sensor was set to 20–400 kHz. The peak definition time (PDT), hit definition time (HDT) and hit locking time (HLT) were set to 50 μs, 100 μs and 300 μs, respectively, according to the characteristics of BFRPC, which ensured the integrity and accuracy of AE signal acquisition [28].

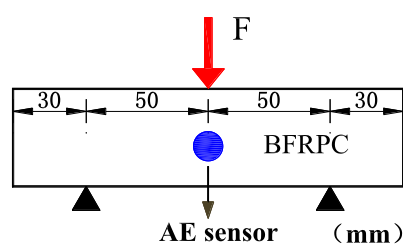


Figure 3. Flexural test and sensor layout. BFRPC, Basalt fiber reactive powder concrete.

4. Discussion

4.1. Workability and Mechanical Properties

The mechanical properties of the nine studied BFRPC are presented in Table 5.

Table 5. Mechanical properties of the studied BFRPC.

Mix	BF1	BF2	BF3	BF4	BF5	BF6	BF7	BF8	BF9
Fluidity (mm)	124	139	154	161	150	139	166	152	155
Compressive strength (MPa)	129.6	109.5	86.4	121.1	131.8	98.8	120.1	136.6	129.4
Flexural strength (MPa)	13.6	11.6	10.8	9.9	13.1	12.2	11.7	12.6	11.9

The fluidity properties of the nine studied mixes are shown in Figure 4. The experimental results show, as expected, the W/B ratio is the most significant factor affecting the workability of BFRPC. The content of free water in the mixture increased with the growth of water–binder ratio, which improved the fluidity of concrete by 10–12%. However, as shown in Figure 4, the increase of mineral admixtures (SF and QS) content carried a 7–14% fluidity penalty. Due to the large specific surface area, the tiny silica fume particles would absorb the free water in the slurry, which led to a decrease in the fluidity of the mixture. On the other hand, the addition of QS played a stable supporting role in the mixture, enhancing the adhesive property of cementitious materials, and increasing the friction force between the fibers and the aggregate particles, which worsened the workability. However, it is evident from Figure 4 that, in the case of RPC, the presence of basalt fiber did not significantly worsen the fluidity performance.

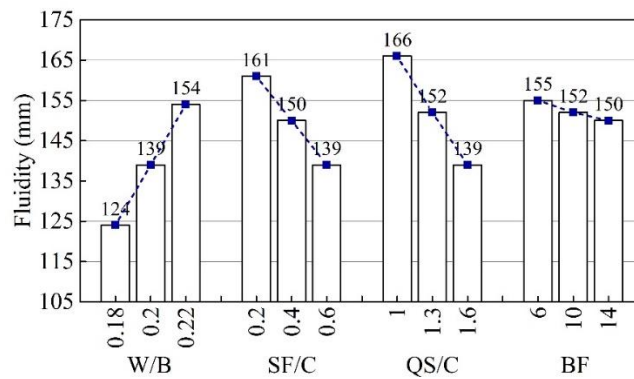


Figure 4. Fluidity of the BFRPC.

The values of the compressive and flexural strength for nine groups of mixes are shown in Figures 5 and 6. With the increase of W/B ratio, the compressive and flexural strength values of BFRPC gradually declined. The high W/B ratio led to the increase of porosity, resulting in the generation of interface weaknesses and the decrease of strength.

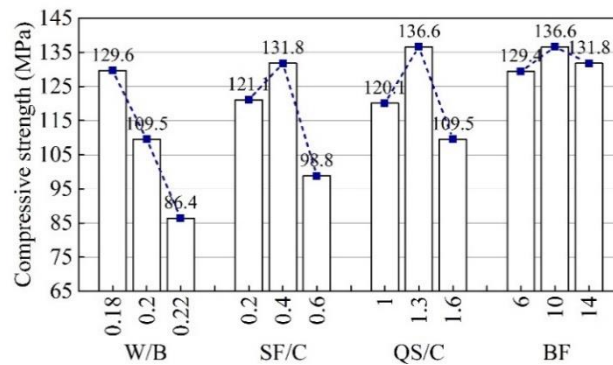


Figure 5. Compressive strength of the BFRPC.

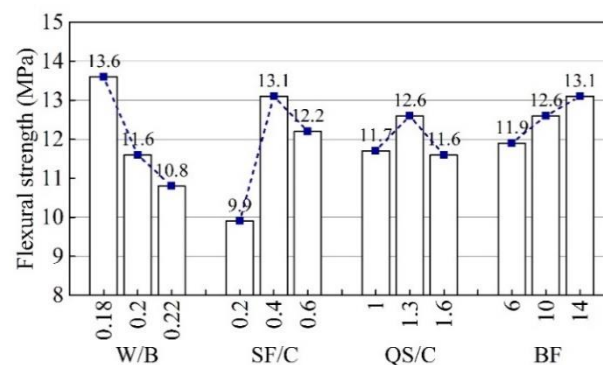


Figure 6. Flexural strength of the BFRPC.

The highest compressive and flexural strength values of 131.8 MPa and 13.1 MPa were obtained when SF/C was 0.4. The hydration reaction of cement generated Ca(OH)_2 , which generated C-S-H gel through the pozzolanic effect with SiO_2 contained in silica fume, filled the internal micro-pores of BFRPC, improved the compactness of the mixture and thus improved the compressive and flexural strength. However, excessive amount of silica fume would limit the immigration of free water in the mixture, which could lead to the occurrence of dry shrinkage. Yinwen Chan [29] proposed a similar effect in strength vanishes when the silica fume content is too high. Initial cracks would be formed inside the matrix, which could damage the integrity of BFRPC materials, resulting in a decrease in the strength.

It can be seen that the most favorable QS/C ratio for BFRPC strength was 1.3. Under this condition, the compressive strength of the material was 136.6 MPa and the flexural strength was 12.8 MPa. As a hard mineral particle, quartz sand could form a stable supporting framework when mixed into the mixture. The uniform filling of cementitious materials in it made good interfacial adhesion between aggregates and cement paste, which improved the density of the concrete matrix. Nevertheless, when too much quartz sand was mixed, the bonding performance between the cementitious materials and aggregates became worse. The resulting weak interfacial transition zone led to the decrease of strength.

For the addition of basalt fiber, the compressive strength was observed to be highest for specimens with fiber content of 10 kg/m³. The fibers uniformly distributed in the matrix could restrain the formation of cracks and share part of the stress, so that the stress around the cracks could be redistributed, which delayed the expansion of micro-cracks in the concrete and improved its mechanical properties. The result agrees with those for basalt fiber reinforced concrete evaluated by Jongsung Sim [8]. However, when the fiber content was too high, it caused the fiber to cluster and could not be dispersed, which reduced its adhesion to the cementitious material. Meanwhile, excessive fiber could lead to accelerated expansion of internal cracks along the direction of fiber distribution in concrete under stress, resulting in strength loss of materials, which was consistent with the results obtained by Ahmet B et al. [30]. In other words, increased content of fibers above the 10 kg/m³ threshold had adverse effects on the compressive strength of specimens. In contrast to the compressive strength, the flexural strength of specimens appeared to increase with increasing fiber content. In the fiber content range of 6–14 kg/m³, the flexural strength increased approximately 10% from 11.9 MPa to 13.1 MPa. This behavior was linked to the connection of fibers across the penetrating cracks generated under bending force, which led to an overall enhanced flexural performance, agreeing with the results obtained by Ayub et al. [11].

In Figure 7, the morphology of a BFRPC specimen after failure is depicted. As can be seen in Figure 7a, the specimen was fully smashed with several vertical penetrating cracks appearing inside under compressive load. In the process of experiment, when the load reached 50% of the ultimate load, the obvious cracking sound began to appear. Then, at the stage of loading up to 70–80% of the ultimate load, the cracking sound was concentrated until the specimen finally breaks. The specimen was broken into two parts as the crack propagated from the bottom surface to the top under flexural load. It can be seen in Figure 7b that the fracture surface of specimen was neat and the internal structure of the specimen was compact.

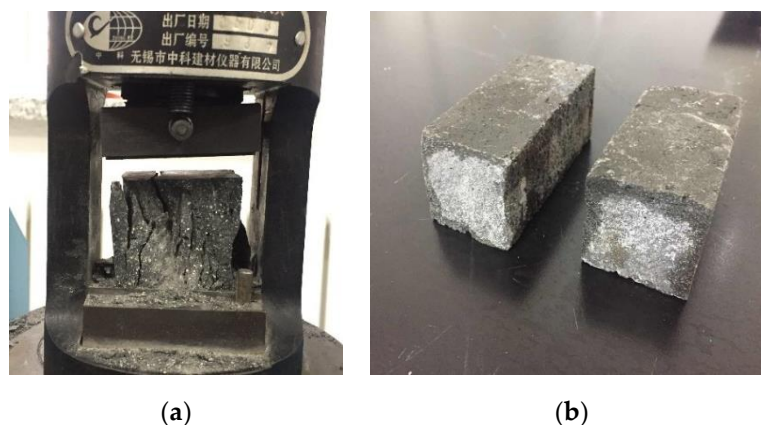


Figure 7. Failure morphology of BFRPC: (a) compressive mode; and (b) flexural mode.

4.2. Acoustic Emission Results

4.2.1. Total AE Hits

It is known that the fracture process of concrete could be confirmed by the analysis of AE characteristic parameters [31]. The AE data for the three groups BF9, BF8, and BF5 were selected for analysis to study the characteristics of BFRPC fracture process with different basalt fiber content.

The ultimate flexural strength loads were normalized and divided into ten load levels. In Figure 8, the cumulative AE hits and energy vs. load level of three groups are depicted. As can be seen in the figure, the cumulative AE hits and the cumulative energy have positive correlation with basalt fiber content. This is because the AE activities associated with fiber pull-out and the pulling out events will increase with the increase of fiber content.

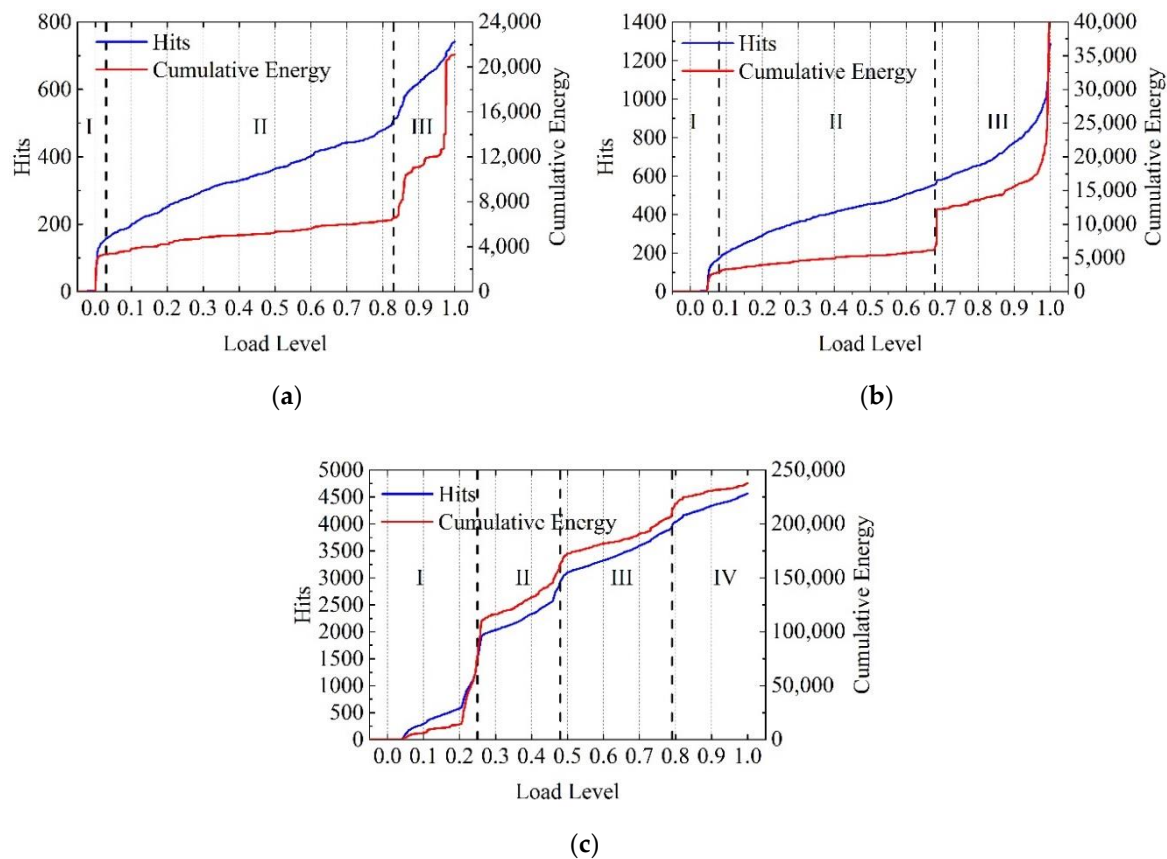


Figure 8. History curves of load level versus cumulative AE features: (a) basalt fiber content of 6 kg/m^3 ; (b) basalt fiber content of 10 kg/m^3 ; and (c) basalt fiber content of 14 kg/m^3 .

As shown in Figure 8a,b, when the fiber content was 6 kg/m^3 and 10 kg/m^3 , the fracture process of specimens could be divided into three stages according to the variation trend of the cumulative curves. In Figure 8a, the explosion of cumulative energy was recorded at 80% load level; the value of cumulative energy grew from 6000 to 20,000 during the third stage. However, the steady increase of cumulative AE hits indicated that the signal strength generated in the final failure stage was relatively large. When the fiber content was 10 kg/m^3 , it can be seen in Figure 8b that the critical point of the third stage was at the load level of 70%. At that moment, the cumulative energy value increased by nearly 100%, and then mutation occurred again when it increased to 20,000, representing the ultimate failure of the specimen. In Figure 8c, it is shown that addition of basalt fibers up to 14 kg/m^3 led to considerable different trend in fracture process, which could be divided into four stages according to the slope change of curves. Most AE events were activated by measurement noise, which explained the small increase in cumulative energy at load level below 0.2. It can be seen that many AE hits were recorded at load level ranging from 0.2 to 0.25, accompanied by an abrupt increase in energy. This behavior was linked to the production of initial cracks that released great energy, which was reported by Giulio Siracusano [17]. When the loading was further increased above 0.25 threshold, the growth trend of cumulative parameters tended to be gentle, indicating that the fracture inside the specimen had entered the stable expansion stage. In contrast to the above two cases, the cumulative

parameter curves tended to be horizontal in the final stage, ranging from load level 0.8 to the collapse of specimen, related to the addition of basalt fibers, which led to an enhancement of toughness.

The AE amplitude value of BFRPC specimens is shown in Figure 9. It can be seen in the figure that the AE amplitude value has a great correlation with the damage stage, which was divided according to cumulative hits and cumulative energy. Sudden increases in amplitude and number of AE signals were observed at the boundaries of each stage. This behavior is also reported in the literature for structure using the AE technique [32]. As shown in Figure 9a,b, at the stage of stable fracture propagation (Stage II), AE amplitude ranged 40–60 dB; at the boundary of Stages II and III, the amplitude reached more than 70 dB; when macro fracture occurred, the amplitude reached a peak of more than 90 dB. As shown in Figure 9c, most of the signals had high amplitude values above 55 dB, which fluctuated with the increase of load. At the critical points of the damage stages, the peak amplitude of more than 75 dB was observed, which was accompanied by the increase of signal quantity. After entering Stage IV, the amplitude value and number of signals were significantly reduced, and, with the amplitude reaching above 75 dB, the specimen was finally fractured.

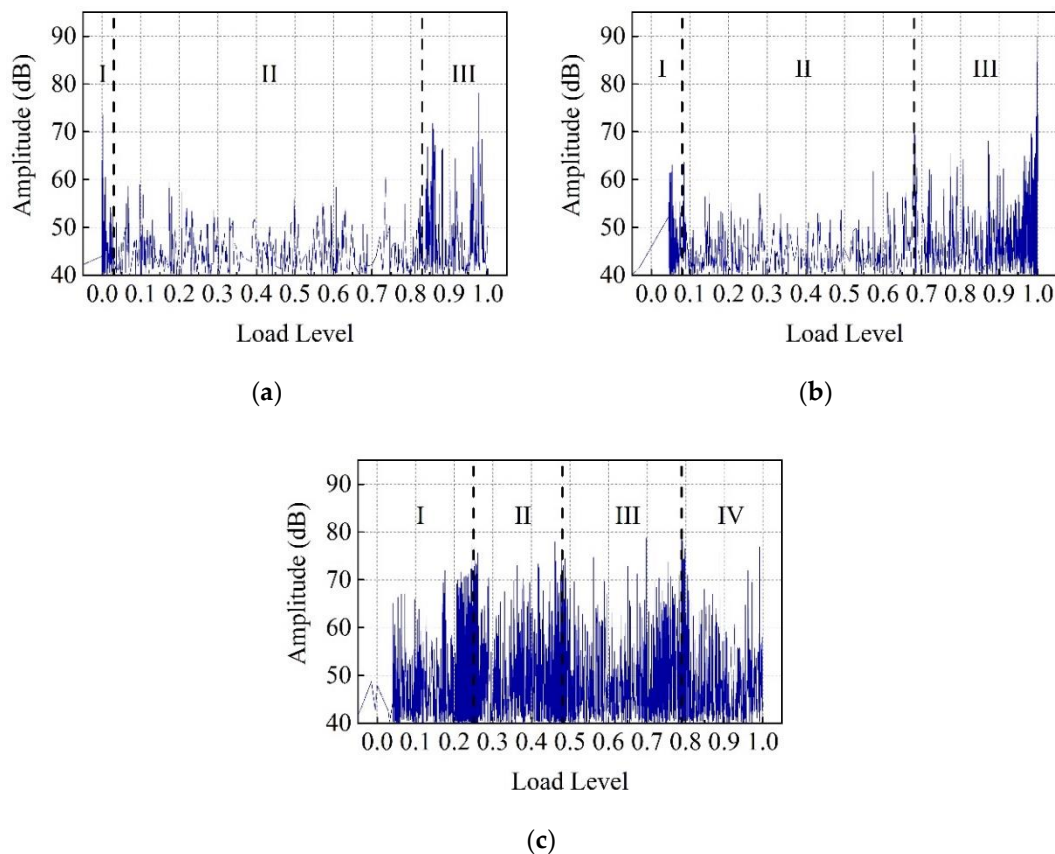


Figure 9. Distribution of amplitude: (a) basalt fiber content of 6 kg/m³; (b) basalt fiber content of 10 kg/m³; and (c) basalt fiber content of 14 kg/m³.

4.2.2. Investigation of Fracture Mode

Previous studies have shown that RA and AF values are the key parameters to characterize the fracture mode of concrete materials. Comparing with shear cracks, tensile cracks led to higher AF and lower RA. The fracture mode of BFRPC under flexural condition was studied by the dynamic changes of parameters throughout the loading process.

Figure 10a–c depicts the change of RA and AF vs. load level for specimens under three fiber contents. To reduce the scattering and show the trend clearly, each point on the curves is the moving average of the recent 50 hits. It can be seen in the figure that the specimen with fiber content of

6 kg/m³ exhibited the lowest RA and the highest AF, respectively, within the range of 50–90 ms/V and 200–800 kHz. When the fiber content increased to 14 kg/m³, RA and AF were obtained, respectively, in the ranges of 70–120 ms/V and 200–600 kHz. Due to the bridging effect of the fibers, the propagation of micro-cracks within the specimens was restricted, and the tensile crack split into different shear cracks. The inclusion of more fibers led to the increase of RA and the decrease of AF, which was associated with the dominance of shear mode in the fracture process. As can be seen in the figure, the moving average curves fluctuated several times in the loading process, which was related to the dynamic fracture of the specimen. The abrupt change of RA and AF values could significantly reflect the transformation of fracture mode, which is consistent with the results obtained by Soulioti et al. [33]. As shown in Figure 10a,b, the average frequency had a sustained downward trend throughout the loading process. The RA rose sharply in the final failure stage, indicating that shear mode dominated the failure of specimens. In Figure 10c, RA and AF values were in a state of constant fluctuation, which meant that the further increase of fiber content led to the existence of shear failure throughout the fracture process. The shift from tensile mode to shear mode was expressed by the increase of RA to above 90 ms/V and the drop of AF to approximately 300 kHz.

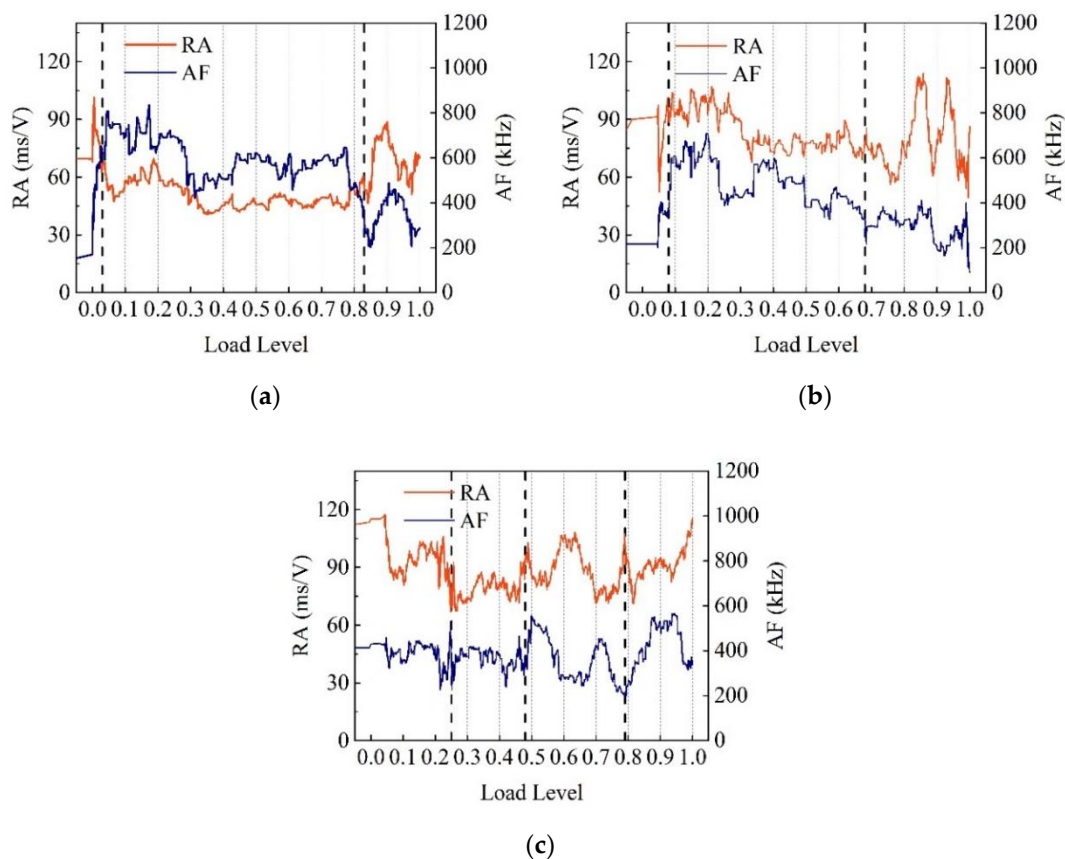


Figure 10. Moving average of RA and average frequency: (a) basalt fiber content of 6 kg/m³; (b) basalt fiber content of 10 kg/m³; and (c) basalt fiber content of 14 kg/m³.

The variation trend of cumulative RA and AF vs. load level in flexural test is illustrated in Figure 11. It can be observed that RA and AF always maintained a similar growth trend during the loading process, indicating that the coupling effect of tensile mode and shear mode existed in the flexural test. For RA and AF with the basalt fiber content of 6 kg/m³, AF fluctuated slightly with no obvious rise or fall during the test, while RA increased sharply within the load level of 0.8–1.0 until the failure of specimen. It revealed that the shear mode dominated the critical failure of specimen after entering the final failure stage. As for the fiber content of 10 kg/m³, RA and AF changed more gently, which was attributed to the increased toughness of specimens by adding fiber. When the fiber content

was further increased to 14 kg/m^3 , RA and AF showed basically the same variation trend and were correlated with the defined fracture stage. As shown in Figure 11c, several sharp rises existed within load level of 0.1–0.5 and the growth trend slowed down from load level 0.5 to 1. The addition of fibers made the tensile fractures generated in the early stage split into several shear fractures, leading to the increase of acoustic emission activities.

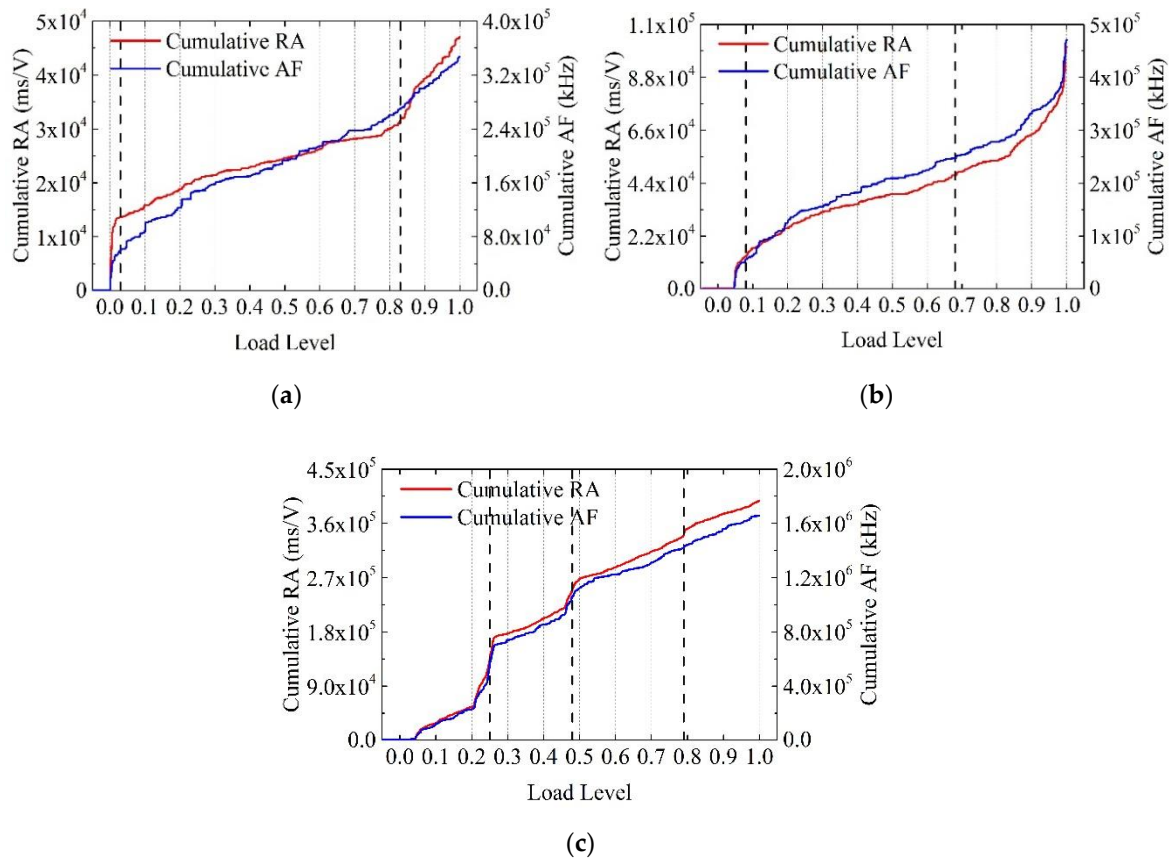


Figure 11. Cumulative RA and average frequency: (a) basalt fiber content of 6 kg/m^3 ; (b) basalt fiber content of 10 kg/m^3 ; and (c) basalt fiber content of 14 kg/m^3 .

5. Conclusions

The presented study investigated the influence of different mix designs to determine the optimal parameters for the improvement of BFRPC properties, and the effects of basalt fibers on the damage features of concrete was simultaneously discussed. For this purpose, a series of mechanical tests were carried out and AE technique was used to monitor the failure process of BFRPC under flexural stress. The conclusions are as follows:

1. The addition of basalt fibers improved significantly the flexural strength without any negative impact on the workability performance. A slightly lower water to binder ratio had to be used to ensure the strength of materials. The appropriate addition of quartz sand formed a stable micro-support framework and improved the distribution of binders within the matrix. The expected values of quartz sand to binder ratio and the silica fume to cement ratio are 0.4 and 1.3, respectively.
2. The activities of AE signals were proportional to the fiber content. The damage fracture process of BFRPC under flexural stress could be accurately divided based on the slope variability of cumulative AE energy. The value of AE amplitude also symbolized the switch of damage stage, which could be used as an early warning of fracture.

3. The fracture mode of BFRPC under flexural test was gradually dominated by shear with the increase of basalt fiber content. This demonstrated the improvement of the fibers against the weak tensile properties and toughness of concrete. It was shown that AE technology can recognize the fracture patterns of specimens by average frequency and RA value, which could assist the damage assessment.

Further application of AE technology in fiber reinforced UHPC could be achieved by, for instance, the damage source location in the matrix through the use of more AE sensors.

Author Contributions: H.L. conceived of and designed the experiments. S.L. analyzed the data and wrote the paper. P.Z. investigated the experiments. Y.Z. audited the content. Y.J. reviewed the content.

Funding: This research was funded by the Industrial Technology Research & Development Special Project of Jilin Province (2018C042-1); the Transportation Science and Technology Program of Jilin Province (2018-1-9); the Science Technology Development Program of Jilin Province (20180201026SF); and the National Natural Science Foundation of China (11702108).

Acknowledgments: The authors would like to express their appreciation for the anonymous reviewers for their constructive suggestions and comments to improve the quality of the paper.

Conflicts of Interest: The authors declare no conflict of interest.

References

1. Richard, P.; Cheyrezy, M. Composition of reactive powder concretes. *Cem. Concr. Res.* **1995**, *25*, 1501–1511. [[CrossRef](#)]
2. Zdeb, T. Ultra-high performance concrete—Properties and technology. *Bull. Pol. Acad. Sci. Tech. Sci.* **2013**, *61*, 183–193. [[CrossRef](#)]
3. Yunsheng, Z.; Wei, S.; Sifeng, L.; Chujie, J.; Jianzhong, L. Preparation of C200 green reactive powder concrete and its static–dynamic behaviors. *Cem. Concr. Compos.* **2008**, *30*, 831–838. [[CrossRef](#)]
4. Wille, K.; Boisvert-Cotulio, C. Material efficiency in the design of ultra-high performance concrete. *Constr. Build. Mater.* **2015**, *86*, 33–43. [[CrossRef](#)]
5. Ipek, M.; Yilmaz, K.; Sümer, M.; Saribiyik, M. Effect of pre-setting pressure applied to mechanical behaviours of reactive powder concrete during setting phase. *Constr. Build. Mater.* **2011**, *25*, 61–68. [[CrossRef](#)]
6. Bae, B.-I.; Choi, H.-K.; Lee, B.-S.; Bang, C.-H. Compressive Behavior and Mechanical Characteristics and Their Application to Stress-Strain Relationship of Steel Fiber-Reinforced Reactive Powder Concrete. *Adv. Mater. Sci. Eng.* **2016**, *2016*, 1–11. [[CrossRef](#)]
7. Afroughsabet, V.; Biolzi, L.; Ozbakkaloglu, T. High-performance fiber-reinforced concrete: A review. *J. Mater. Sci.* **2016**, *51*, 6517–6551. [[CrossRef](#)]
8. Sim, J.; Park, C.; Moon, D.Y. Characteristics of basalt fiber as a strengthening material for concrete structures. *Compos. Part B Eng.* **2005**, *36*, 504–512. [[CrossRef](#)]
9. Branston, J.; Das, S.; Kenno, S.Y.; Taylor, C. Mechanical behaviour of basalt fibre reinforced concrete. *Constr. Build. Mater.* **2016**, *124*, 878–886. [[CrossRef](#)]
10. Wang, D.; Ju, Y.; Shen, H.; Xu, L. Mechanical properties of high performance concrete reinforced with basalt fiber and polypropylene fiber. *Constr. Build. Mater.* **2019**, *197*, 464–473. [[CrossRef](#)]
11. Ayub, T.; Shafiq, N.; Nuruddin, M.F. Mechanical Properties of High-performance Concrete Reinforced with Basalt Fibers. *Procedia Eng.* **2014**, *77*, 131–139. [[CrossRef](#)]
12. Nair, A.; Cai, C.S. Acoustic emission monitoring of bridges: Review and case studies. *Eng. Struct.* **2010**, *32*, 1704–1714. [[CrossRef](#)]
13. Prem, P.R.; Murthy, A.R. Acoustic emission and flexural behaviour of RC beams strengthened with UHPC overlay. *Constr. Build. Mater.* **2016**, *123*, 481–492. [[CrossRef](#)]
14. Farhidzadeh, A.; Salamone, S.; Luna, B.; Whittaker, A. Acoustic emission monitoring of a reinforced concrete shear wall by b-value-based outlier analysis. *Struct. Health Monit.* **2013**, *12*, 3–13. [[CrossRef](#)]
15. Zhang, X.C.; Shan, W.C.; Zhang, Z.W.; Li, B. AE monitoring of reinforced concrete squat wall subjected to cyclic loading with information entropy-based analysis. *Eng. Struct.* **2018**, *165*, 359–367. [[CrossRef](#)]
16. Sagar, R.V. A parallel between earthquake sequences and acoustic emissions released during fracture process in reinforced concrete structures under flexural loading. *Constr. Build. Mater.* **2016**, *114*, 772–793. [[CrossRef](#)]

17. Siracusano, G.; Lamonaca, F.; Tomasello, R.; Garesci, F.; La Corte, A.; Carni, D.L.; Carpentieri, M.; Grimaldi, D.; Finocchio, G. A framework for the damage evaluation of acoustic emission signals through Hilbert-Huang transform. *Mech. Syst. Signal Process.* **2016**, *75*, 109–122. [[CrossRef](#)]
18. Mhamdi, L.; Schumacher, T. A Comparison Between Time-of-Arrival and Novel Phased Array Approaches to Estimate Acoustic Emission Source Locations in a Steel Plate. *J. Nondestruct. Eval.* **2015**, *34*, 38. [[CrossRef](#)]
19. Aggelis, D.G.; Soulioti, D.V.; Sapouridis, N.; Barkoula, N.M.; Paipetis, A.S.; Matikas, I.E. Acoustic emission characterization of the fracture process in fibre reinforced concrete. *Constr. Build. Mater.* **2011**, *25*, 4126–4131. [[CrossRef](#)]
20. Kurz, J.H.; Grosse, C.U.; Reinhardt, H.W. Strategies for reliable automatic onset time picking of acoustic emissions and of ultrasound signals in concrete. *Ultrasonics* **2005**, *43*, 538–546. [[CrossRef](#)] [[PubMed](#)]
21. Mpalaskas, A.C.; Matilzas, T.E.; Van Hemelrijck, D.; Papakitsos, G.S.; Aggelis, D.G. Acoustic emission monitoring of granite under bending and shear loading. *Arch. Civ. Mech. Eng.* **2016**, *16*, 313–324. [[CrossRef](#)]
22. Carpinteri, A.; Lacidogna, G.; Accornero, F.; Mpalaskas, A.C.; Matikas, T.E.; Aggelis, D.G. Influence of damage in the acoustic emission parameters. *Cem. Concr. Comp* **2013**, *44*, 9–16. [[CrossRef](#)]
23. Tragazikis, I.K.; Dassios, K.G.; Exarchos, D.A.; Dalla, P.T.; Matikas, T.E. Acoustic emission investigation of the mechanical performance of carbon nanotube-modified cement-based mortars. *Constr. Build. Mater.* **2016**, *122*, 518–524. [[CrossRef](#)]
24. Ohno, K.; Ohtsu, M. Crack classification in concrete based on acoustic emission. *Constr. Build. Mater.* **2010**, *24*, 2339–2346. [[CrossRef](#)]
25. National Standard of the People's Republic of China. *Test Methods for Cement and Concrete for Highway Engineering (JTG E30-2005)*; Ministry of Transport of the People's Republic of China: Beijing, China, 2006.
26. National Standard of the People's Republic of China. *Method of Testing Cements-Determination of Strength (GB/T 17671-1999)*; Quality and Technology Supervision Bureau of the People's Republic of China: Beijing, China, 1999.
27. Fan, X.Q.; Hu, S.W.; Lu, J.; Wei, C.J. Acoustic emission properties of concrete on dynamic tensile test. *Constr. Build. Mater.* **2016**, *114*, 66–75.
28. Kim, J.S.; Lee, K.S.; Cho, W.J.; Choi, H.J.; Cho, G.C. A Comparative Evaluation of Stress-Strain and Acoustic Emission Methods for Quantitative Damage Assessments of Brittle Rock. *Rock Mech. Rock Eng.* **2015**, *48*, 495–508. [[CrossRef](#)]
29. Chan, Y.W.; Chu, S.H. Effect of silica fume on steel fiber bond characteristics in reactive powder concrete. *Cem. Concr. Res.* **2004**, *34*, 1167–1172. [[CrossRef](#)]
30. Kizilkanat, A.B.; Kabay, N.; Akyuncu, V.; Chowdhury, S.; Akca, A.R. Mechanical properties and fracture behavior of basalt and glass fiber reinforced concrete: An experimental study. *Constr. Build. Mater.* **2015**, *100*, 218–224. [[CrossRef](#)]
31. Behnia, A.; Chai, H.K.; Yorikawa, M.; Momoki, S.; Terazawa, M.; Shiotani, T. Integrated non-destructive assessment of concrete structures under flexure by acoustic emission and travel time tomography. *Constr. Build. Mater.* **2014**, *67*, 202–215. [[CrossRef](#)]
32. Li, D.S.; Du, F.Z. Monitoring and evaluating the failure behavior of ice structure using the acoustic emission technique. *Cold Reg. Sci. Technol.* **2016**, *129*, 51–59. [[CrossRef](#)]
33. Soulioti, D.; Barkoula, N.M.; Paipetis, A.; Matikas, T.E.; Shiotani, T.; Aggelis, D.G. Acoustic emission behavior of steel fibre reinforced concrete under bending. *Constr. Build. Mater.* **2009**, *23*, 3532–3536. [[CrossRef](#)]

